A Journal of the Gesellschaft Deutscher Chemiker

Angewandte International Edition

GDCh

Chemie

www.angewandte.org

Accepted Article

Title: Elegant Synthesis of CuS@CoS2 Double-Shelled Nanoboxes with Enhanced Sodium Storage Properties

Authors: Xiong-Wen (David) Lou

To be cited as: *Angew. Chem. Int. Ed.* 10.1002/anie.201902583
Angew. Chem. 10.1002/ange.201902583

Link to VoR: http://dx.doi.org/10.1002/anie.201902583
http://dx.doi.org/10.1002/ange.201902583

WILEY-VCH

10.1002/anie.201902583

Elegant Synthesis of CuS@CoS_2 Double-Shelled Nanoboxes with Enhanced Sodium Storage Properties

Yongjin Fang, Bu Yuan Guan, Deyan Luan, and Xiong Wen (David) Lou[*]

[*] Dr. Y. J. Fang, Dr. B. Y. Guan, Dr. D. Y. Luan, Prof. X. W. Lou

School of Chemical and Biomedical Engineering, Nanyang Technological University, 62 Nanyang Drive, Singapore 637459, Singapore

Email: xwlou@ntu.edu.sg; davidlou88@gmail.com

Webpage: http://www.ntu.edu.sg/home/xwlou/

Abstract

Metal sulfides have received considerable interest for efficient sodium storage owing to their high capacity and decent redox reversibility. However, the poor rate capability and fast capacity decay greatly hinder their practical application in sodium-ion batteries. Herein, an elegant multi-step templating strategy has been developed to rationally synthesize hierarchical double-shelled nanoboxes with the CoS_2 nanosheet-constructed outer shell supported on the CuS inner shell. With the structural and compositional advantages, these hierarchical CuS@CoS_2 nanoboxes manifest boosted electrochemical properties with high capacity, outstanding rate capability, and long cycle life.

Keywords: nanosheets, nanoboxes, CoS_2, CuS, sodium-ion batteries

10.1002/anie.201902583

Sodium-ion batteries (SIBs) have aroused increasing interest as a promising candidate for large-scale electric energy storage in view of their overwhelming merits of both cost and natural abundance compared to the established lithium-ion battery systems.[1-8] Developing efficient anode materials is highly desirable to promote the practical implementation of SIBs.[9, 10] Due to the high capacity and good electrochemical reversibility, various metal sulfides such as CoS_x, CuS_x, SnS_x, FeS_x have been reported for sodium storage.[11-19] However, most of them suffer from poor conductivity and large volume change during electrochemical reactions, which cause limited rate and cycling performance. Rational design in nanostructure and carbon modification are two effective ways to address these issues thus to enhance the electrochemical performance. For example, construction of hybrid nanostructures for electrodes has been proposed as an effective strategy to enhance the sodium storage properties, owing to the synergetic effects from different components.[20, 21]

Hierarchical hollow configurations assembled by low-dimensional nanoscale building blocks show promising properties in high-performance SIBs.[22-26] The hollow structure with high surface area can effectively accommodate the strain during electrochemical reactions and facilitate the full infiltration of electrolyte. And the low-dimensional nanosized building units can offer significantly decreased electron/ion transport pathways, leading to better rate performance. Notwithstanding a lot of progress achieved, fabrication of metal sulfides with complex nanoarchitectures and chemical compositions with enhanced sodium storage properties is less reported.

Herein, we demonstrate the rational design and construction of hierarchical $CuS@CoS_2$ double-shelled nanoboxes (DSNBs) by taking advantage of the unique reactivity of Cu_2O. The multi-step synthesis process of the $CuS@CoS_2$ DSNBs is schematically depicted in **Figure 1**. First, a shell of $Co(OH)_2$ nanosheets is grown on Cu_2O nanocubes by carefully manipulating the balance of the coordinating etching rate toward the Cu_2O template and precipitating rate of the $Co(OH)_2$ nanosheets. Afterward, the obtained $Cu_2O@Co(OH)_2$ core-shell nanocubes are selectively sulfurized by a proper amount of Na_2S solution at room temperature to get the $Cu_2O@CuS@Co(OH)_2$ nanocubes. Then, the

Cu_2O core in the Cu_2O@CuS@$Co(OH)_2$ is selectively removed with a $Na_2S_2O_3$ solution to obtain the hierarchical CuS@$Co(OH)_2$ nanoboxes. Lastly, the resultant CuS@$Co(OH)_2$ nanoboxes are further transformed to CuS@CoS_2 DSNBs via a solvothermal sulfidation process. The as-obtained CuS@CoS_2 DSNBs simultaneously combine the structural and compositional design rationales as advanced anodes for SIBs. As expected, the as-synthesized CuS@CoS_2 DSNBs demonstrate improved electrochemical performance with high reversible capacity, decent rate performance and long cyclability.

Cu_2O nanocubes synthesized through a reduction method are employed as the starting templates. Field-emission scanning electron microscopy (FESEM) images show that the as-synthesized Cu_2O nanocubes are quite homogeneous with an average particle size of around 650 nm (**Figure 2**a and Figure S1a,b, Supporting Information (SI)). The transmission electron microscopy (TEM) images (Figure 2e and Figure S1c, SI) indicate the solid nature of these nanocubes. X-ray diffraction (XRD) (Figure S1d, SI) and energy-dispersive X-ray spectroscope (EDX) analysis (Figure S2, SI) further confirm the crystalline structure and phase purity of the Cu_2O. When the Cu_2O nanocubes react with a proper amount of $CoCl_2$ and $Na_2S_2O_3$ for 1.5 min, a shell of $Co(OH)_2$ nanosheets is grown on the Cu_2O nanocubes. A typical FESEM image (Figure 2b) of the as-derived sample demonstrates that the particles still maintain the cubic shape but the surface become extremely rough. TEM images (Figure 2f and Figure S3, SI) reveal that the shell consists of random nanosheets. The evolution of the $Co(OH)_2$ nanosheets on the Cu_2O nanocubes can be attributed to the controlled coordinating etching and precipitating reaction.[27]

A subsequent sulfidation process is conducted by the mild treatment of core-shell Cu_2O@$Co(OH)_2$ nanocubes with an appropriate amount of Na_2S at room temperature. FESEM (Figure 2c) and TEM (Figure 2g and Figure S4, SI) images reveal that the morphology of the as-formed product exhibits small variation compared to the core-shell Cu_2O@$Co(OH)_2$ nanocubes. However, the EDX result of the as-derived product (Figure S5, SI) reveals the existence of S element,

10.1002/anie.201902583

which should come from CuS formed through the reaction between surficial oxidized CuO and S^{2-} ions.[28, 29] The selective sulfidation of copper oxide cores in the $Cu_2O@Co(OH)_2$ nanocubes is because of the ultralow solubility product constant (K_{sp}) of CuS, leading to remarkably high binding force between Cu^{2+} and S^{2-} ions in solution. The as-prepared $Cu_2O@CuS@Co(OH)_2$ nanocubes are then transformed into $CuS@Co(OH)_2$ nanoboxes by selectively etching Cu_2O out. The cubic structure is well retained after the elimination of the Cu_2O core (Figure 2d). And a distinct interior cavity can be obviously discerned in the nanocube (Figure 2h and Figure S6a,b, SI), and the ultrathin nanosheets on the outer shell are unaltered during the etching process (Figure S6c, SI). The EDX spectrum (Figure S7, SI) shows the presence of Cu, Co, S, and O elements, confirming the composition of $CuS@Co(OH)_2$.

Through a sulfidation treatment in thioacetamide solution, the $CuS@Co(OH)_2$ nanoboxes are converted to $CuS@CoS_2$ DSNBs. All the diffraction peaks in the XRD pattern are readily identified as cubic CoS_2 and hexagonal CuS (Figure S8a, SI), and the EDX result indicates that these $CuS@CoS_2$ DSNBs have a Co/Cu molar ratio of 1:0.84 (Figure S8b, SI). The FESEM images (**Figure 3**a,b and Figure S9a, SI) demonstrate that the $CuS@CoS_2$ DSNBs inherit the hierarchical cubic structure. Magnified FESEM image clearly shows the hierarchical shells, which are composed of randomly assembled nanosheets (Figure 3c). The well-defined hollow configuration of the $CuS@CoS_2$ DSNBs is verified by TEM (Figure 3d) and FESEM (Figure S9b, SI) studies. The hierarchical nanosheets show some shrink (Figure 3e and Figure S9c, SI) compared to those of the $CuS@Co(OH)_2$ nanoboxes. A closer examination on the shell of an individual $CuS@CoS_2$ DSNB reveals that no visible inter-shell gap can be discerned (Figure S9d, SI), suggesting that the CoS_2 nanosheets are strongly anchored on the CuS inner shell. The typical lattice fringe (Figure 3f) of the outermost nanosheet has an interplanar distance of 0.32 nm, which is consistent with the d-value of (111) plane of cubic CoS_2.

10.1002/anie.201902583

In addition, by controlling the coordinating etching and precipitating reaction time to 6 min, yolk-shelled Cu_2O-$Co(OH)_2$ nanocubes can be synthesized (Figure S10a,b, SI). Accordingly, well-defined double-shelled CuS-$Co(OH)_2$ nanoboxes (Figure S10c,d, SI) and their derived double-shelled nanoboxes (here denoted as CuS-CoS_2 DSNBs) can be obtained through similar sulfidation and etching processes. The CuS-CoS_2 DSNBs exhibit similar composition (Figure S11, SI) and preserve the hierarchical nanobox structure (Figure **4**a and Figure S12a, SI). TEM images (Figure 4d and Figure S10e,f, SI) and FESEM image (Figure S12b, SI) further confirm that the as-obtained CuS-CoS_2 DSNBs hold a unique shell-in-shell hollow configuration, in which an apparent gap between the outer and inner shells can be observed. The enlarged view of one CuS-CoS_2 DSNB (Figure S12c, SI) reveals that the outer shell is constructed by CoS_2 nanosheets, while the inner shell consists of CuS nanoparticles. Moreover, single-shelled CoS_2 nanoboxes (denoted as CoS_2 SSNBs) (Figure S13, SI) and single-shelled CuS nanoboxes (denoted as CuS SSNBs) (Figure S14, SI) can be obtained through the sulfidation of $Co(OH)_2$ nanoboxes (Figure S15 and Figure S16a,b, SI) and Cu_2O nanocubes (Figure S1, SI), respectively. The CoS_2 SSNBs exhibit hierarchical nanosheet-assembled single-shelled nanoboxes (Figure 4b,e and Figure S16c,d, SI), while the CuS SSNBs are constructed by nanoparticles with well-defined cube-like morphology (Figure 4c,f and Figure S17, SI).

The electrochemical performance of the CuS@CoS_2 DSNBs are investigated by assembling coin cells. **Figure 5**a shows the representative cyclic voltammetry (CV) curves of the CuS@CoS_2 DSNBs. In the first cathodic scan, a small broad peak at 1.49 V corresponds to the Na^+ ion insertion into the CuS structure,[30, 31] while the sharp reduction peak located at 1.25 V can be assigned to Na^+ ion insertion into CoS_2.[32, 33] Another small peak at 0.95 V may be associated with the structural transformation of the Na_xCuS phases.[34, 35] And the peaks at 0.85 and 0.50 V are ascribed to the conversion of Na_xCoS_2 to Co and Na_2S and the formation of a solid-electrolyte interphase (SEI) film.[36, 37] In the second cathodic scan, two new peaks at 1.91 and 1.49 V emerge, which are ascribed to the Na^+ ion intercalation processes of CuS_x and CoS_x, respectively.[32, 34-36, 38] During the anodic

scans, two peaks at about 1.58 and 2.15 V are associated with deintercalation of Na^+ ions from the Na_xCuS structure,[34, 35, 39] and three peaks at 1.87, 1.96 and 2.07 V represent the reverse processes from Co and Na_2S to the CoS_x.[32, 36, 38] Figure 5b displays the representative galvanostatic discharge-charge curves of the CuS@CoS_2 DSNBs at 0.1 A g^{-1}. Remarkably, the CuS@CoS_2 DSNBs deliver a stable reversible capacity of about 625 mAh g^{-1}, which is higher than those of the CoS_2 SSNBs and CuS SSNBs (Figure S18, SI), and most CoS_x-based anodes.[33, 40-44] The initial CV and discharge-charge curves of CuS@CoS_2 DSNBs show some difference with that of subsequent cycles, which can be ascribed to the structural rearrangement and formation of SEI film in the initial sodiation process.[36, 38, 41]

The rate performance of the CuS@CoS_2 DSNBs, CuS@CoS_2 DSNBs, CoS_2 SSNBs and CuS SSNBs is examined at various current densities. As presented in Figure 5c, the average reversible capacities of CuS@CoS_2 DSNBs are 612, 570, 535, 483, 416, 360 mAh g^{-1} at 0.1, 0.2, 0.3, 0.5, 1, 2 A g^{-1}, respectively. Even at a large current density of 5 A g^{-1}, the CuS@CoS_2 DSNBs can also deliver a high capacity of 304 mAh g^{-1}. In stark contrast, the reversible capacities of the CuS-CoS_2 DSNBs and CoS_2 SSNBs decrease quickly when the current density is increased. Notably, the CuS SSNBs exhibit superior rate capability without obvious capacity decay at high current densities but with relatively low specific capacities. The outstanding rate performance of the CuS@CoS_2 DSNBs can also be confirmed by the discharge-charge curves at different current densities (Figure 5d). Furthermore, the CuS@CoS_2 DSNBs also show good cycling performance. Of note, 79% of the initial capacity is retained after 500 cycles at a current density of 0.5 A g^{-1} (Figure 5e). Impressively, the CuS@CoS_2 DSNBs also exhibit excellent cyclic stability at 0.3 A g^{-1} (Figure S19, SI). Moreover, CuS@CoS_2 DSNBs still largely retain their nanobox structures after cycling (Figure S20, SI). For comparison, the capacities of the CuS-CoS_2 DSNBs and CoS_2 SSNBs drop rapidly, while the CuS SSNBs exhibit superior cyclability (Figure 5e). The stable cyclability of the CuS@CoS_2 DSNBs is also better than most CoS_x-based electrodes.[32, 38, 41, 43-45] To explain the outstanding rate performance

10.1002/anie.201902583

of the CuS@CoS_2 DSNBs, a kinetics analysis based on CV test is performed (Figure S21, SI). The results suggest the characteristics of capacitance-controlled kinetics of the CuS@CoS_2 DSNBs. The high capacitive contribution of CuS@CoS_2 DSNBs is mainly due to the hierarchical nanosheet-on-nanobox configuration, which provides a large surface for the adsorption and desorption of Na^+ ions during the repeated (de)sodiation processes.[46, 47]

The outstanding sodium storage properties of these CuS@CoS_2 DSNBs may be ascribed to the distinctive hierarchical hollow configuration and synergistic effect of the CoS_2 nanosheets supported on CuS nanoboxes. Specifically, the primary nanosheet building blocks could decrease the diffusion path of electrons/Na^+ ions to accelerate the reaction kinetics. Both the hollow architecture and nanosheet subunits could efficiently accommodate the mechanical strain during repeated discharge-charge processes. The CuS backbone can enhance the electronic conductivity of the CuS@CoS_2 DSNBs thus to effectively boost the charge transfer process (Figure S22, SI). Besides, the double-shelled structure could improve the structural integrity of the active materials, leading to remarkable enhanced cycling performance.

In summary, we have proposed a delicate templating strategy for the effective synthesis of hierarchical double-shelled nanoboxes with the CoS_2 nanosheet-assembled outer shell supported on the CuS inner nanobox for efficient sodium storage. The rational synthetic strategy, involving a controlled coordinating etching and precipitating reaction and subsequent sulfidation and etching processes, can effectively tailor the structures and compositions of the final nanoarchitectures. Owing to the distinctive structural and compositional advantages, the CuS@CoS_2 double-shelled nanoboxes demonstrate boosted electrochemical performance for sodium storage with high reversible capacity (625 mAh g^{-1}), outstanding rate performance (304 mAh g^{-1} at 5 A g^{-1}), and excellent cycling stability (79% capacity retention after 500 cycles). This work may inspire further potentials for the design and construction of hierarchical hollow configurations with great complexity for diverse applications.

Acknowledgments

X. W. L. acknowledges the funding support from the National Research Foundation (NRF) of Singapore via the NRF investigatorship (NRF-NRFI2016-04).

References

[1] Y. Fang, X.-Y. Yu, X. W. Lou, *Angew. Chem. Int. Ed.* **2017**, *56*, 5801.

[2] Y. You, H.-R. Yao, S. Xin, Y.-X. Yin, T.-T. Zuo, C.-P. Yang, Y.-G. Guo, Y. Cui, L.-J. Wan, J. B. Goodenough, *Adv. Mater.* **2016**, *28*, 7243.

[3] Y. Li, Y. Lu, C. Zhao, Y.-S. Hu, M.-M. Titirici, H. Li, X. Huang, L. Chen, *Energy Storage Mater.* **2017**, *7*, 130.

[4] C. Chen, Y. Wen, X. Hu, X. Ji, M. Yan, L. Mai, P. Hu, B. Shan, Y. Huang, *Nat. Commun.* **2015**, *6*, 6929.

[5] Y. Fang, Q. Liu, L. Xiao, Y. Rong, Y. Liu, Z. Chen, X. Ai, Y. Cao, H. Yang, J. Xie, C. Sun, X. Zhang, B. Aoun, X. Xing, X. Xiao, Y. Ren, *Chem* **2018**, *4*, 1167.

[6] L. Zhuang, *Acta Phys.-Chim. Sin.* **2017**, *33*, 1271.

[7] M. S. Kim, E. Lim, S. Kim, C. Jo, J. Chun, J. Lee, *Adv. Funct. Mater.* **2017**, *27*, 1603921.

[8] Y. Fang, L. Xiao, J. Qian, X. Ai, H. Yang, Y. Cao, *Nano Lett.* **2014**, *14*, 3539.

[9] W. Luo, F. Shen, C. Bommier, H. Zhu, X. Ji, L. Hu, *Acc. Chem. Res.* **2016**, *49*, 231.

[10] H. Xie, X. Tan, E. J. Luber, B. C. Olsen, W. P. Kalisvaart, K. L. Jungjohann, D. Mitlin, J. M. Buriak, *ACS Energy Lett.* **2018**, *3*, 1670.

[11] Y. Xiao, S. H. Lee, Y.-K. Sun, *Adv. Energy Mater.* **2016**, *7*, 1601329.

[12] Y. Fang, L. Xiao, Z. Chen, X. Ai, Y. Cao, H. Yang, *Electrochem. Energ. Rev.* **2018**, *1*, 294.

[13] Z. Hu, Q. Liu, S.-L. Chou, S.-X. Dou, *Adv. Mater.* **2017**, *29*, 1700606.

[14] X. Xiong, G. Wang, Y. Lin, Y. Wang, X. Ou, F. Zheng, C. Yang, J.-H. Wang, M. Liu, *ACS Nano* **2016**, *10*, 10953.

[15] Y. Liu, X.-Y. Yu, Y. Fang, X. Zhu, J. Bao, X. Zhou, X. W. Lou, *Joule* **2018**, *2*, 725.

[16] Z. Liu, T. Lu, T. Song, X.-Y. Yu, X. W. Lou, U. Paik, *Energy Environ. Sci.* **2017**, *10*, 1576.

[17] Y. Xiao, D. Su, X. Wang, S. Wu, L. Zhou, Y. Shi, S. Fang, H.-M. Cheng, F. Li, *Adv. Energy Mater.* **2018**, *8*, 1800930.

[18] X. Y. Yu, X. W. Lou, *Adv. Energy Mater.* **2017**, *8*, 1701592.

[19] Y. Fang, Z. Chen, L. Xiao, X. Ai, Y. Cao, H. Yang, *Small* **2018**, *14*, 1703116.

[20] Y. Zheng, T. Zhou, C. Zhang, J. Mao, H. Liu, Z. Guo, *Angew. Chem. Int. Ed.* **2016**, *55*, 3408.

[21] J. Wang, J. Liu, H. Yang, D. Chao, J. Yan, S. V. Savilov, J. Lin, Z. X. Shen, *Nano Energy* **2016**, *20*, 1.

[22] B. Chen, Y. Meng, F. Xie, F. He, C. He, K. Davey, N. Zhao, S.-Z. Qiao, *Adv. Mater.* **2018**, *30*, 1804116.

[23] Z. Liu, X.-Y. Yu, X. W. Lou, U. Paik, *Energy Environ. Sci.* **2016**, *9*, 2314.

[24] Y. Fang, X.-Y. Yu, X. W. Lou, *Adv. Mater.* **2018**, *30*, 1706668.

[25] S. Wang, Y. Fang, X. Wang, X.-W. Lou, *Angew. Chem. Int. Ed.* **2019**, *58*, 760.

[26] P. He, Y. Fang, X.-Y. Yu, X. W. Lou, *Angew. Chem. Int. Ed.* **2017**, *56*, 12202.

[27] J. Nai, Y. Tian, X. Guan, L. Guo, *J. Am. Chem. Soc.* **2013**, *135*, 16082.

[28] M. Pang, H. C. Zeng, *Langmuir* **2010**, *26*, 5963.

[29] S.-Q. Liu, H.-R. Wen, G. Ying, Y.-W. Zhu, X.-Z. Fu, R. Sun, C.-P. Wong, *Nano Energy* **2018**, *44*, 7.

[30] J. Y. Park, S. J. Kim, J. H. Chang, H. K. Seo, J. Y. Lee, J. M. Yuk, *Nat. Commun.* **2018**, *9*, 922.

[31] H. Li, Y. Wang, J. Jiang, Y. Zhang, Y. Peng, J. Zhao, *Electrochim. Acta* **2017**, *247*, 851.

[32] Z. Shadike, M.-H. Cao, F. Ding, L. Sang, Z.-W. Fu, *Chem. Commun.* **2015**, *51*, 10486.

[33] Y. Pan, X. Cheng, Y. Huang, L. Gong, H. Zhang, *ACS Appl. Mater. Interfaces* **2017**, *9*, 35820.

[34] J. Li, D. Yan, T. Lu, W. Qin, Y. Yao, L. Pan, *ACS Appl. Mater. Interfaces* **2017**, *9*, 2309.

[35] H. Park, J. Kwon, H. Choi, D. Shin, T. Song, X. W. D. Lou, *ACS Nano* **2018**, *12*, 2827.

[36] F. Han, T. Lv, B. Sun, W. Tang, C. Zhang, X. Li, *RSC Adv.* **2017**, *7*, 30699.

[37] Z. Li, W. Feng, Y. Lin, X. Liu, H. Fei, *RSC Adv.* **2016**, *6*, 70632.

[38] X. Liu, K. Zhang, K. Lei, F. Li, Z. Tao, J. Chen, *Nano Res.* **2016**, *9*, 198.

[39] J.-S. Kim, D.-Y. Kim, G.-B. Cho, T.-H. Nam, K.-W. Kim, H.-S. Ryu, J.-H. Ahn, H.-J. Ahn, *J. Power Sources* **2009**, *189*, 864.

[40] Z. Chen, R. Wu, M. Liu, H. Wang, H. Xu, Y. Guo, Y. Song, F. Fang, X. Yu, D. Sun, *Adv. Funct. Mater.* **2017**, *27*, 1702046.

[41] C. Wu, Y. Jiang, P. Kopold, P. A. van Aken, J. Maier, Y. Yu, *Adv. Mater.* **2016**, *28*, 7276.

[42] S. Peng, X. Han, L. Li, Z. Zhu, F. Cheng, M. Srinivansan, S. Adams, S. Ramakrishna, *Small* **2016**, *12*, 1359.

[43] L. Zhou, K. Zhang, J. Sheng, Q. An, Z. Tao, Y.-M. Kang, J. Chen, L. Mai, *Nano Energy* **2017**, *35*, 281.

[44] Q. Zhou, L. Liu, Z. Huang, L. Yi, X. Wang, G. Cao, *J. Mater. Chem. A* **2016**, *4*, 5505.

[45] Y. Xiao, J.-Y. Hwang, I. Belharouak, Y.-K. Sun, *Nano Energy* **2017**, *32*, 320.

[46] P. Simon, Y. Gogotsi, B. Dunn, *Science* **2014**, *343*, 1210.

[47] D. Chao, C. Zhu, P. Yang, X. Xia, J. Liu, J. Wang, X. Fan, S. V. Savilov, J. Lin, H. J. Fan, Z. X. Shen, *Nat. Commun.* **2016**, *7*, 12122.

10.1002/anie.201902583

Figures and Captions

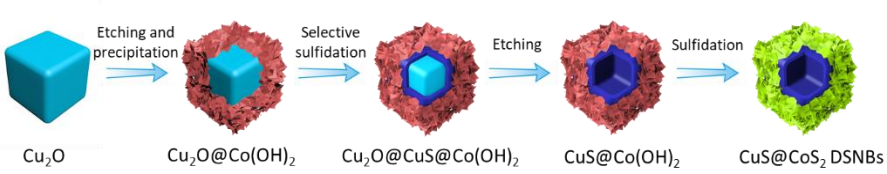

Figure 1. Schematic illustration of the synthetic process of $CuS@CoS_2$ DSNBs.

10.1002/anie.201902583

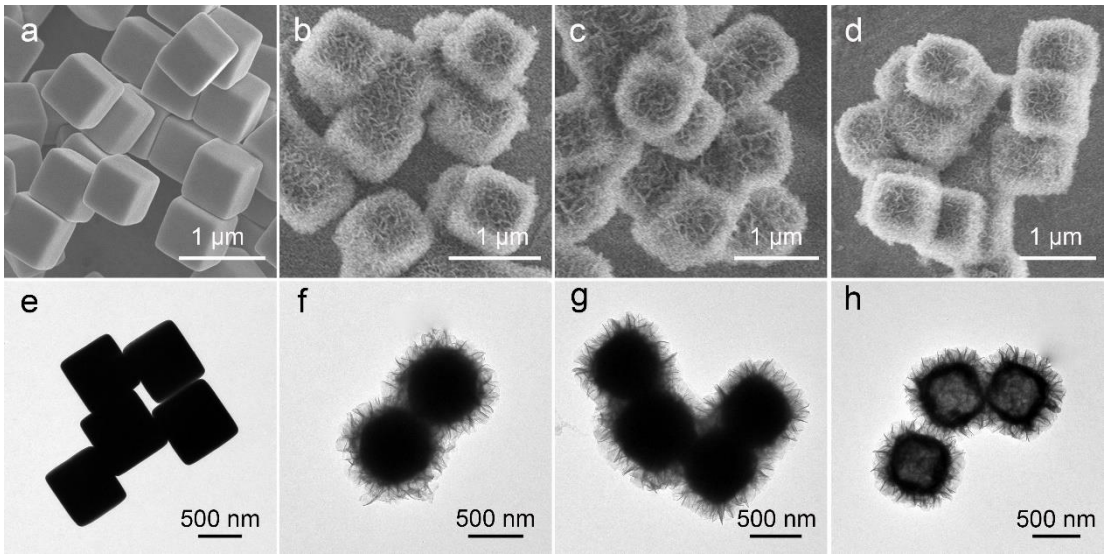

Figure 2. (a-d) FESEM images and (e-h) TEM images of the (a, e) Cu_2O nanocubes, (b, f) core-shell $Cu_2O@Co(OH)_2$ nanocubes, (c, g) $Cu_2O@CuS@Co(OH)_2$ nanocubes, (d, h) $CuS@Co(OH)_2$ nanoboxes.

10.1002/anie.201902583

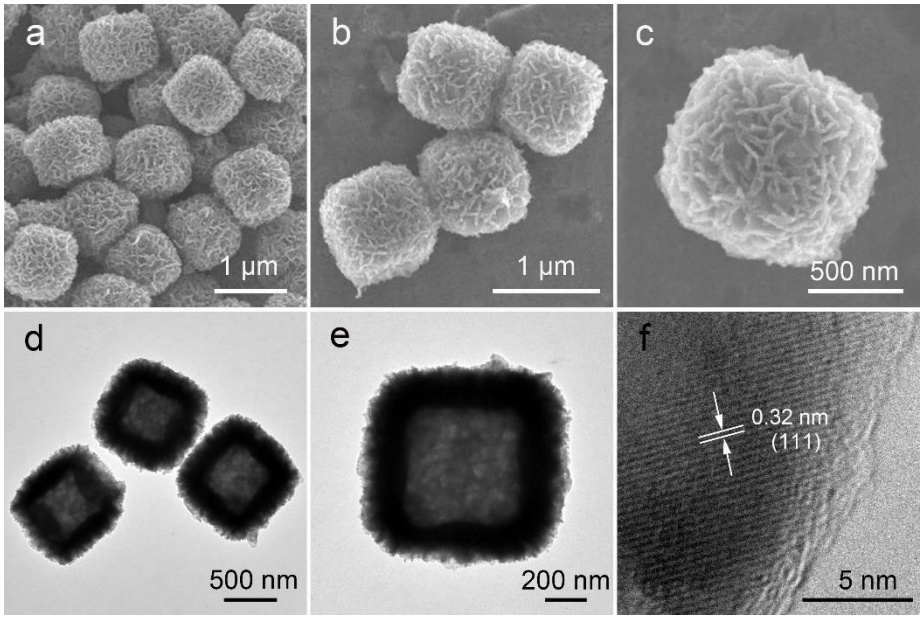

Figure 3. (a-c) FESEM images, (d, e) TEM images, and (f) HRTEM image of the CuS@CoS_2 DSNBs.

10.1002/anie.201902583

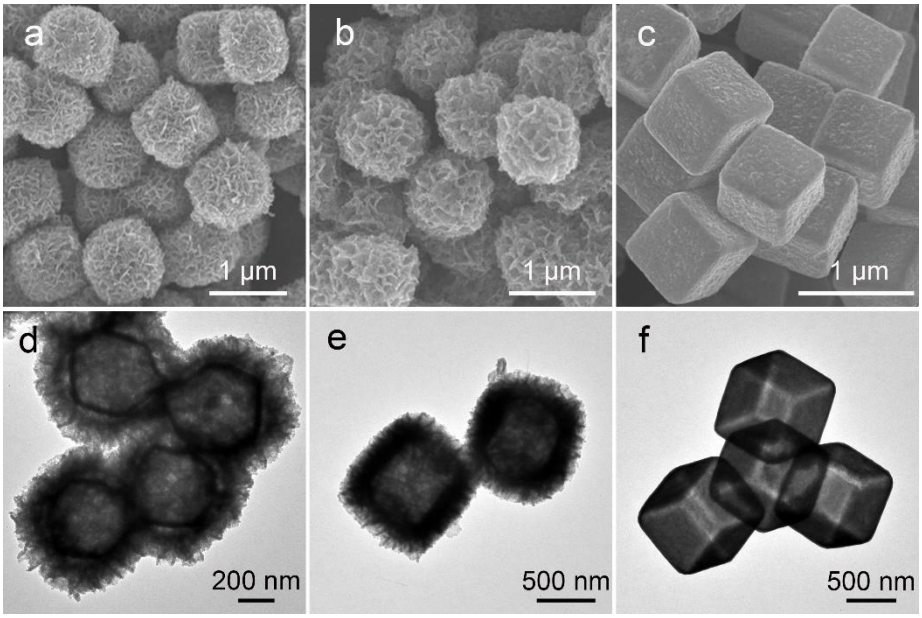

Figure 4. (a-c) FESEM images and (d-f) TEM images of the (a, d) CuS-CoS_2 DSNBs, (b, e) CoS_2 SSNBs, and (c, f) CuS SSNBs.

10.1002/anie.201902583

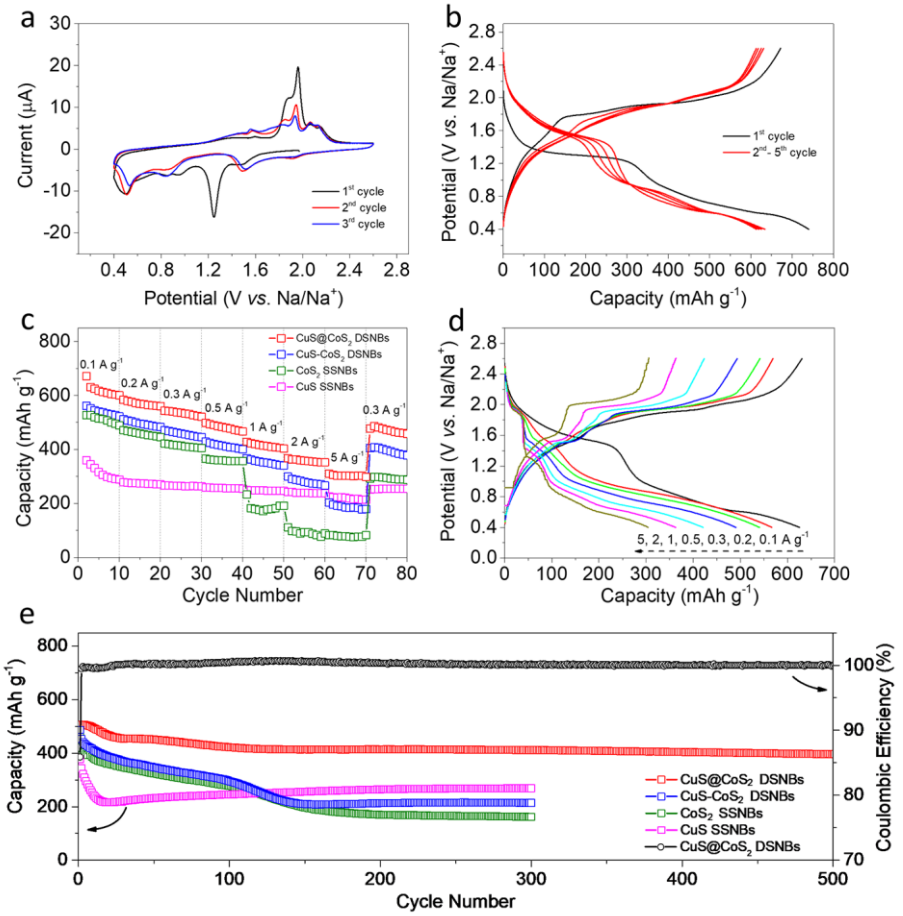

Figure 5. (a) The 1st to 3rd cyclic voltammograms of the CuS@CoS_2 DSNBs at a scan rate of 0.1 mV s^{-1}. (b) Typical discharge-charge voltage profiles of the CuS@CoS_2 DSNBs at a current density of 0.1 A g^{-1}. (c) Rate performance of the CuS@CoS_2 DSNBs, CuS-CoS_2 DSNBs, CoS_2 SSNBs and CuS SSNBs, and (d) The corresponding discharge-charge voltage profiles of the CuS@CoS_2 DSNBs at various current densities. (e) Cycling performance of the CuS@CoS_2 DSNBs, CuS-CoS_2 DSNBs, CoS_2 SSNBs and CuS SSNBs at a current density of 0.5 A g^{-1}, and the corresponding Coulombic efficiency of the CuS@CoS_2 DSNBs.

10.1002/anie.201902583

for Table of Content Entry

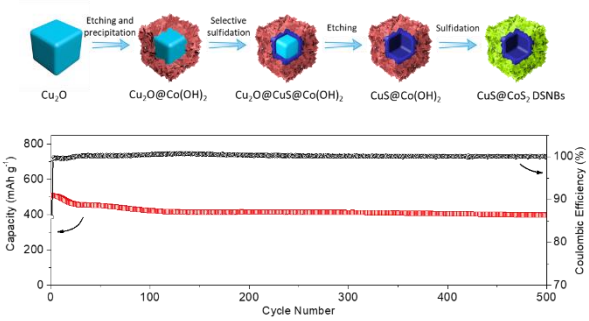

Double-shelled CuS@CoS_2 nanoboxes composed of an outer shell of hierarchical CoS_2 nanosheets supported on the inner CuS nanobox are synthesized by a delicate template-engaged strategy using Cu_2O nanocubes as the starting material. With the structural and compositional merits, these hierarchical CuS@CoS_2 nanoboxes exhibit attractive electrochemical properties as an anode material for sodium-ion batteries.